OPTICAL MICROACTUATION IN PIEZOCERAMICS

[1]Sarita Thakoor[a], P. Poosanaas[c], J. M. Morookian[a], A. Yavrovian[a], L. Lowry[a], N. Marzwell[a], J. Nelson[b], R. R. Neurgaonkar[b], and Kenji Uchino[c]

[a]Jet Propulsion Laboratory, California Institute of Technology, PASADENA, CA 91109
[b]Rockwell Science Center, Thousand Oaks, CA 91360
[c]Pennsylvania State University, University Park, PA 16802

ABSTRACT:

Optically/electrically operable flexible film microactuators that can offer upto two orders higher efficiency of photonic to mechanical conversion compared to ceramic actuators are conceptualized. A polarized ceramic wafer of non-centrosymmetric perovskite ferroelectric ABO_3 compounds, such as lead lanthanum zirconate titanate (PLZT), when exposed to an illumination (~350 to 400 nm wavelength) close to the bandgap energy, can generate a large photovoltage (~1.0 kV/mm) across its length, and by the inverse piezoelectric effect cause the piezoceramic wafer to deflect in the direction away from the illumination. The optical actuation effect in piezoceramic wafers is investigated as a function of thickness, composition, and surface roughness. Such flexible microactuators would enable a new generation of micro-electro-mechanical and micro-opto-mechanical systems where the actuation will not be restricted by the clamping effect due to the rigid substrate as in the current silicon based micromachined structures. To deposit the piezoceramic film directly onto a flexible substrate, the substrate must have high temperature stability, high strength (Young's Modulus ~ 4.9×10^{10} N/m^2), a close match of thermal coefficients of expansion with the piezoceramic film, and a tailorable crystal orientation in order to provide a desired template for growth of oriented PLZT.
This paper also presents a comparison of a variety of flexible substrate films and fibers and our recent results on polybenzoxazole (PBO), a polymeric candidate for a flexible high temperature substrate. Variation of the properties of PBO as a function of temperature are also presented.

1. INTRODUCTION

Optically/electrically operable "flexible actuators" that can offer upto two orders higher efficiency of photonic to mechanical conversion are conceptualized[1,2]. A polarized ceramic wafer of non-centrosymmetric perovskite ferroelectric ABO_3 compounds, such as lead lanthanum zirconate titanate (PLZT), when exposed to an illumination (~350 to 400 nm wavelength) close to the bandgap energy, can generate[3] a large photovoltage (~1.0 kV/mm) across its length, and by the *inverse piezoelectric* effect cause the piezoceramic wafer to deflect in the direction away from the illumination. The hypothesis is that if the

[1] Further Author Information:
Sarita Thakoor (correspondence): Email: sarita.thakoor @ jpl.nasa.gov; Telephone: (818) 354-0862;
MS 303-308, Jet Propulsion Laboratory, 4800 Oak Grove Drive, Pasadens, CA 91109

absorption of the illumination occurs in at the most ~ tens of microns thick surface layer of the piezoelectric material facing the illumination, the photovoltage generation is expected[3] to be entirely located in this thin top skin layer. Using a film thickness equal to this penetration depth ensures that the entire film is active. In a ceramic typically ~ 200 micron thick, almost 90 % of the bulk is an inactive mass to be bent/deflected. In films, therefore using the analytical treatment for electrically operated bimorphs used by Moulson[4] , we expect the deflection to be ~ 500 times larger. This arises because of the 100 times lower thickness and the 5 times higher electrical field strength.

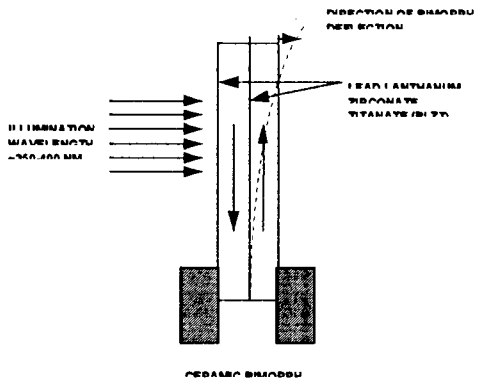

ceramic thickness: 200 micron

(a)

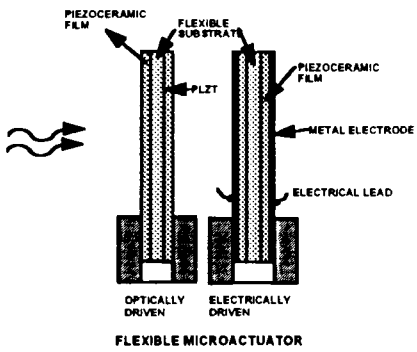

film thickness: 2 micron

(b)

Figure 1

Figure 1a and figure 1b compare a ceramic bimorph and a flexible film bimorph.
The table 1 shows the projected parameters of improvement. The numbers in this table are calculated based on using a 200 micron thick typical ceramic wafer as the current state of the art and a 2 micron thick film as the projected flexible film bimorph. Such a film bimorph activated with 5 V will have~ 25 times higher[1,2,5] energy density than the ceramic bimorph that requires ~ 100 V. In turn, although the net force output from the bimorph will be 20 % of that from the ceramic, the force /volume will be five times higher. Correspondingly, in the case of optical actuation, the film bimorph is projected to deliver force output 2-20 times that of the ceramic due to the enhancement in conversion efficiency (expected value ~ 1% - 10%). This is expected with illumination intensity an order magnitude lower than that currently used for the ceramics. This will result in an enhancement of force per unit power by 20 to 200 times. Obtaining the optical performance enhancement in input photonic power to output mechanical force will provide a substantially enhanced flexible film actuator as indicated. Demonstration of this matrix of improvement will set the foundation for photonic control of mechanical motion and flexible actuators.

TABLE 1: COMPARISON OF BULK PIEZOCERAMIC ACTUATOR WITH PROJECTED PERFORMANCE OF FLEXIBLE FILM ACTUATOR

		Current Status Ceramic Actuator	Projected Improvement Film Actuator
ELECTRICAL ACTUATION PARAMETERS	Thickness	200 microns	2 microns: Thickness reduced, material tailored
	Operating Voltage	100 V	5 V : Operational voltage reduced
	Energy Density	1X	25 X : Inherent advantage of reduced thickness
	Deflection	1X	500X enhancement for film actuator
	Force/Volume	1X	5X enhancement for film actuator
OPTICAL ACTUATION PARAMETERS	Optical Power	80 mW/cm^2	8 mW/ cm^2 : Illumination Intensity
	Power Ratio	10X	1X
	Photonic to Mechanical Conversion Efficiency	0.1%	1% - 10% : significant enhancement in overall efficiency
	Force/Energy	1X	2X to 20X : Multifold enhancement in the film actuator
	Force/Power	1X	20X to 200X

2. WIDE APPLICATION DOMAIN

The applications[1,2,6] of the optical actuation effect could be classified into two broad classes:

1. Microactuation &
2. Microsensing

This direct conversion of photonic to mechanical motion will lead to following potential applications:

a. optical shape control of structures
b. a new alternative mechanism for converting solar energy directly into mechanical motion for planetary exploration (for example on Mars where conversion devices that can be operated from the low cryogenic temperature ~ -125°C to + 55°C are required. Piezoceramic based this novel converter will be uniquely suited for such operational cycling with its wide temperature range of operation and excellent cyclability)
c. direct corrective control in adaptive optics/interferometry,
d. optical micropositioning,

e. solar tracking actuator/shutter for self alignment of the spacecraft to the sun for optimal power generation or station keeping using solar sails,
f. optically controlled valves for medical as well as space applications,
g. photophones, that convert flashes of light directly into sound.
h. optically controlled microrobots

On the other hand, potential microsensing applications include:

a. a variety of tunable sensors for incident radiation (UV, visible etc.) based on a direct calibration of the deflection as a function of incident radiation intensity, and
b. indirect microsensors based on calibration of the photodeflection in presence of the device "loading" (e.g. change in the deflection when the device is "loaded" with condensing moisture (microhygrometer) or incident interstellar dust (microbalance)).

3. EXPERIMENTAL PROCEDURE:

PLZT (3/52/48) ceramics with 3 at.% La and a Zr/Ti ratio of 52/48 and 0.5 at.% WO_3 as dopant were prepared by the conventional oxide mixing process, where $PbCO_3$, La_2O_3, ZrO_2, TiO_2 and dopants (WO_3) were mixed in the proper ratio and ball milled for 48 h. Subsequently, the slurry was dried, calcined at 950°C for 10 h, and sintered at 1270°C for 2 h. The detail of the process has been reported by Poosanaas et al[7].

PLZT samples were cut to the standard size of 4x5 mm^2 with various thickness 50 μm -1 mm. Samples were polished, electroded with silver paste and electrically poled along the length (5 mm) direction in silicone oil at 120°C under a 2 kV/mm for 10 min. Photovoltaic measurements were done by using a high-input-impedance electrometer (Keithley 617) while the photostriction was measured by a displacement sensor (LVDT, Millitron model 1301). A high pressure mercury lamp (Ushio Electric USH-500D) was used as a light source. The lamp radiation was passed through an IR blocking filter and a UV bandpass filter to obtain a monochromatic beam with a maximum strength around 370 nm wavelength. The 4x5 mm^2 polished surface of the sample was illuminated. The experimental set-up for photovoltaic and photostrictive measurements was reported in an earlier paper al[7,8].

Bimorph and unimorph samples are illuminated on either of their faces by ultra-violet light. The samples are clamped at one end. The displacement that results at the far end of the cantilever formed by the body of the sample itself is measured by an optical deflection measurement and/or an eddy current sensor.

The optical deflection measurement is accomplished by affixing to the free end of the sample a thin mirrored glass slide. A He-Ne laser beam is directed onto the mirror at an angle, and a spot from the deflected beam is observed on a grid several meters from the sample. When the sample flexes due to UV radiation, the change in the angle of the sample surface to the He-Ne beam is observed as a displacement of the observed spot (magnified by the large distance arm of the observation grid). This serves as a good visual measure of the displacement, although the accuracy of measurement in terms of

deflection and time dynamics measurement is limited to ~ 25 microns and visual discrimination.

The eddy current sensor measurement offers a much higher resolution ~ 2 microns and could allow in conjunction with a fast switch, time dynamics study of the temporal response down to fraction of a microsecond since the contact less electronic measurement does not load the sample mechanically. The sample is prepared by affixing a small square of aluminum foil to the free end of the sample so as to form a suitable target for the eddy current sensor. When the sample flexes due to UV radiation, the foil target is moved toward or away from the eddy current sensor. This displacement causes a change in the inductive field and consequently a change in voltage from the sensor which is recorded by an oscilloscope, allowing fast displacements to be observed and recorded.

4. RESULTS

i. Investigation of flexible substrates:

To deposit the piezoceramic film directly onto a flexible substrate, the substrate must have high temperature stability, high strength (Young's Modulus ~ 4.9×10^{10} N/m^2), a close match of thermal coefficients of expansion with the piezoceramic film, and a tailorable crystal orientation in order to provide a desired template for growth of oriented PZT. Earlier work has shown[9] that ferroelectric PZT could be crystallized at ~ 550°C. Recently[10] polybenzoxazole (PBO) has been validated at JPL to work well up to ~ 550°C and extensively characterized for operation at 460°C. Table 2 & 3 provide a comparison of a variety of substrate films and fibers. PBO stands out as the leading candidate for its high tensile strength, high Young's Modulus, low heat shrinkage and coefficients of thermal expansion and hygroscopic expansion to provide such a high temperature substrate for forming flexible microactuators by this technique. PBO is a conjugated aromatic heterocyclic liquid crystalline polymer (LCP) with a chemical structure as shown in Figure 2.

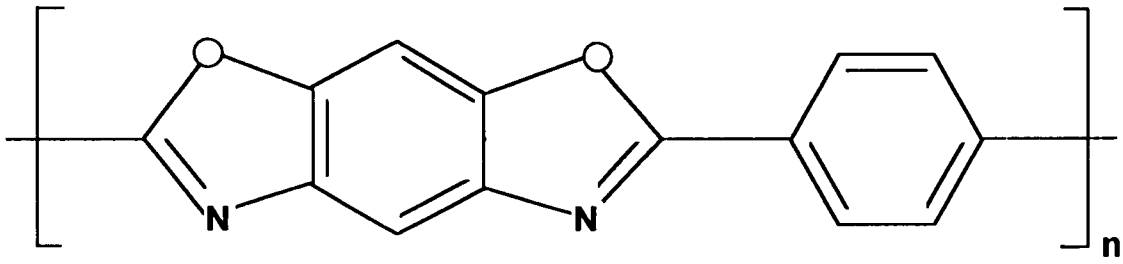

CIS-PBO

Figure 2. Chemical Structure of PBO

PROPERTY	UNIT	KAPTON	ARAMID	PET	PEN	PBO
DENSITY	g/cm^3	1.420	1.500	1.395	1.355	1.54
MELTING TEMP	°C	NONE	NONE	263	272	NONE
GLASS TRANSITION TEMP	°C	350	280	68	113	NONE
YOUNG'S MODULUS	kg/mm^2	300	1000-2000	500-850	650-1400	4900
TENSILE STRENGTH	kg/mm^2	18	50	25	30	56-63
TENSILE ELONGATION	%	70	60	150	95	1-2
LONG-TERM HEAT STABILITY	°C	230	180	120	155	>300
HEAT SHRINKAGE (200°C x % min)	%	0.1	0.1	5-10	1.5	<0.1
COEFFICIENT OF THERMAL EXPANSION	ppm/°C	20	15	15	13	-2
COEFFICIENT OF HYGROSCOPIC EXPANSION	ppm/% RH	20	18	10	10	0.8
MOISTURE ABSORPTION	%	2.9	1.5	0.4	0.4	0.8

Table 2: Comparison of a variety of polymeric films

PROPERTY	PBO	PBO HIGH MODULUS	ARAMID	STEEL	SPECTRA® (HDPE)	CARBON (HI-TENSILE)	GLAS (S-2)
TENSILE STRENGTH (ksi)	820	800	400-500	250	435	500-700	665
TENSILE MODULUS (Msi)	25-30	40-45	10-25	29	25	30-40	12.6
COMPRESSIVE STRENGTH (ksi)	40	65	65	250	10	300-400	>150
ELONGATION, BREAK (%)	3.0	1.5	1.5-4.0	2.0	3.5	1.5-2.0	5.4
DENSITY (g/cc)	1.56	1.56	1.44	7.86	0.97	1.8-1.9	2.4
SPECIFIC TENSILE STRENGTH (ksi)	525	510	280-350	32	450	270-380	280
SPECIFIC TENSILE MODULUS	16	26	7-18	4	26	16-22	5
LIMITING OXYGEN INDEX (LOI: %)	56	56	30		19	50-65	

Table 3: Comparative data for high performance fibers

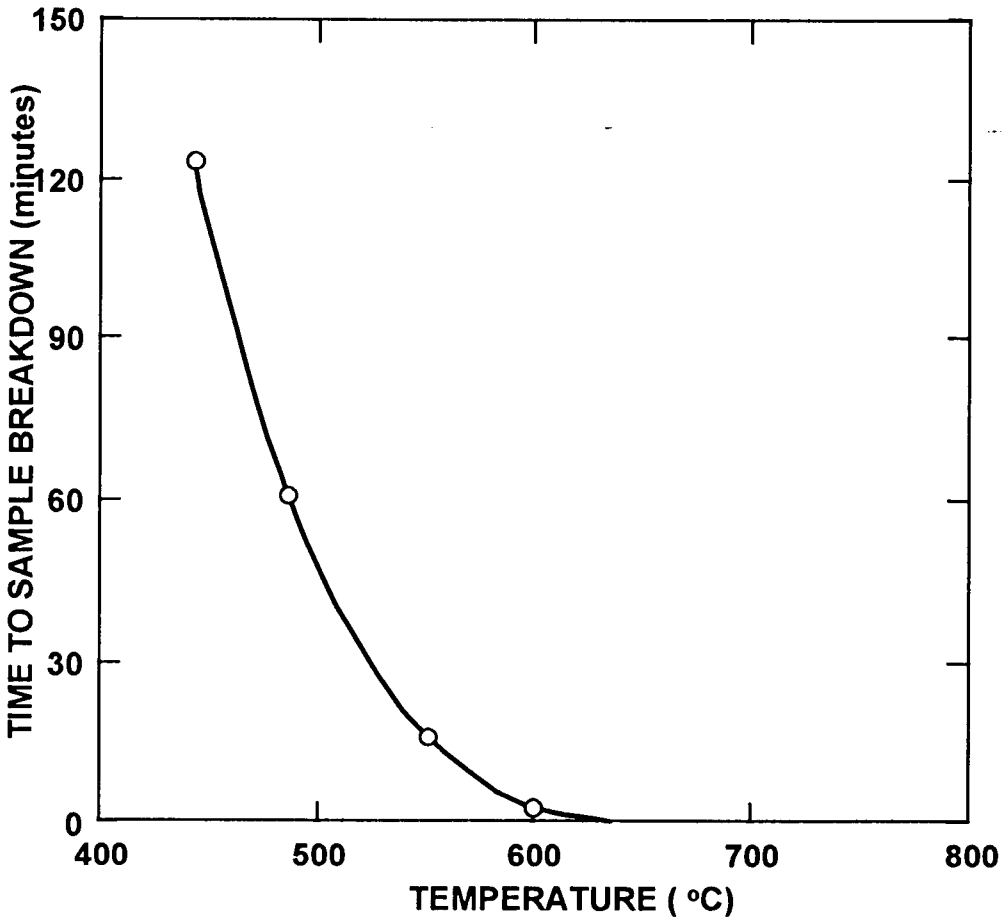

Figure 3: Time to sample breakdown of PBO as a function of temperature

The chemical synthesis of PBO results in a LCP solution that is processed to fiber or film by various techniques. The high strength and superior physical properties of PBO are due to the rod-like nature of the PBO molecule (Figure 3) and the orientation that can be built into the Polymer film. PBO film's self-reinforcing microstructure results in a "molecular fabric" with properties comparable to those of advanced, fiber-reinforced materials, but without the drawbacks of distinct fiber and matrix components. This polymer has no melting point or glass transition temperature.

In conclusion, this comparative analysis suggests that PBO in general is a good candidate for flexible substrates. Figure 3 further shows the dependence of time to PBO sample breakdown as a function of temperature. It is clear, that this substrate is stable for extensive operation at temperatures of 460°C or lower. Therefore, to deposit an active film of PLZT, another challenge needs to be overcome. The crystallization temperature of the piezoceramic film needs to be brought down to about 450°C or the crystallization be obtained by very rapid bursts of high temperatures through rapid laser annealing.

ii. Crystallization Temperature for PZT:

Figure 4 shows the X-ray diffraction patterns of a PZT(52/48) thin film mounted on the hot stage of a Siemens Allis D-500 diffractometer taken progressively at temperatures from

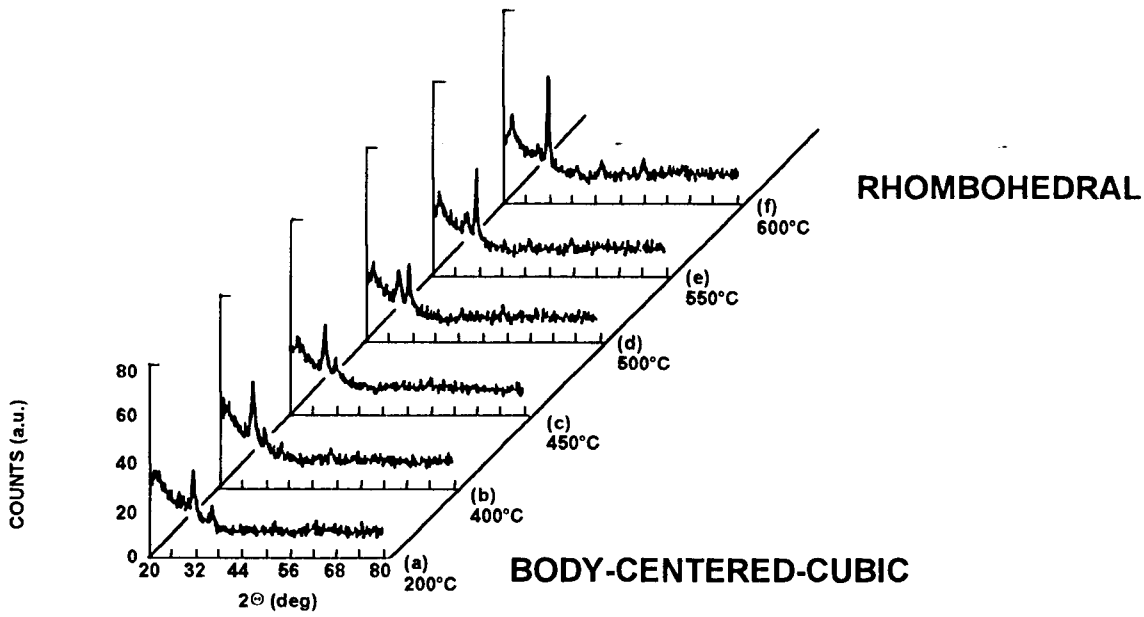

Figure 4: X-Ray Diffraction Patterns From A PZT Film Annealed In Air At Different Temperatures

200°C to 600°C. The x-ray diffraction study was performed in reflection mode using CuKα radiation. As deposited, the film exhibits predominantly the lead structure. In fig. 4, the x-ray pattern at 200°C still predominantly shows all the lead lines. However, at about 400°C the solid state reaction leading to formation of the lead oxides initiates, as is indicated by the appearance of the (111) line. At about 550°C, the reaction completes to give the rhombohedral phase of lead zirconate titanate, as is evident from the comparison in Fig 3. The additional appearance of the (100) line of the rhombohedral phase signifies this transition clearly. Therefore, it is apparent that in-order to deposit the piezoceramic thin films on PBO (which has been demonstrated to operate repeatably at the highest temperature of 460° C), the crystallization temperature of PZT needs to be brought down by another 100 C. Further, for large structures stretched aircraft grade aluminum foils have worked[11] better than coated polymeric films such as mylar. Therefore, keeping in mind the application of shape control in structures, metallic foil of platinum is being used for this work. The technology for depositing piezoceramic thin films on platinum thin films is known and therefore can be more rapidly transitioned to obtain optimized optically actuating thin films on flexible platinum foils.

iii. Optical actuation as function of sample thickness of PLZT Ceramics:

When a sample is illuminated, the incident radiation is absorbed as it penetrates into the crystal lattice. The amount of light intensity reaching at the thickness 'x' of the sample is given as:

$$I(x) = TI_o e^{(-\alpha x)} \quad (1)$$

where I(x) is the light intensity at thickness 'x', I_o is the incident light intensity , T is the transmittance at the sample surface (78%), and α is the absorption coefficient of the sample.

The absorption coefficient (α) was determined by measuring incident and transmitted light intensity, using a digital power meter (Newport model 815), as a function of sample thickness.

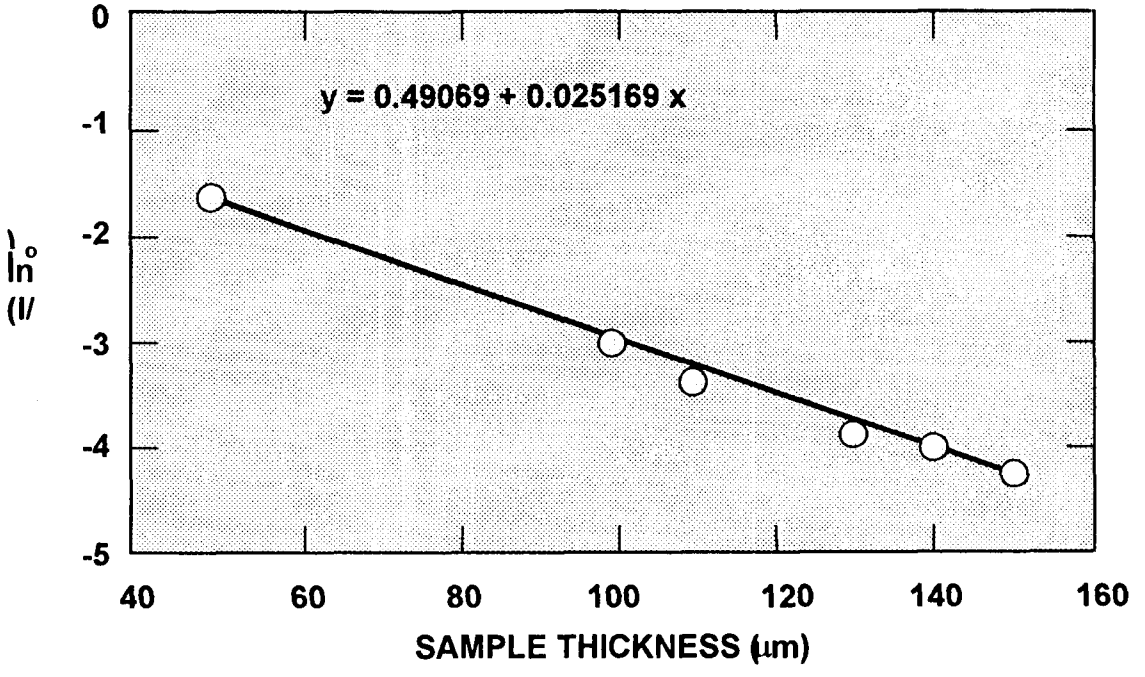

Figure 5: Light intensity as a function of sample thickness

Fig. 5 shows the plot between light intensity as a function of sample thickness. The absorption coefficient, determined from the slope of this plot was found to be 0.0252 μm^{-1}.

In case of thinner sample, there will be substantial intensity 'I' throughout the sample thickness, whereas for thick sample after some distance the intensity 'I' will be very small or negligible. The relationship between light intensity and photocurrent density formulated by Glass[12] given as:

$$J_{ph} = k\alpha I \quad (2)$$

Where J_{ph} is photocurrent density, and k is photovoltaic coefficient. It is apparent from Eq. (2), that the photocurrent will increase with the intensity of radiation, resulting in a

higher photocurrent in the thinner samples. As is expected, photocurrent increases (Fig. 6) with decrease in the sample thickness.

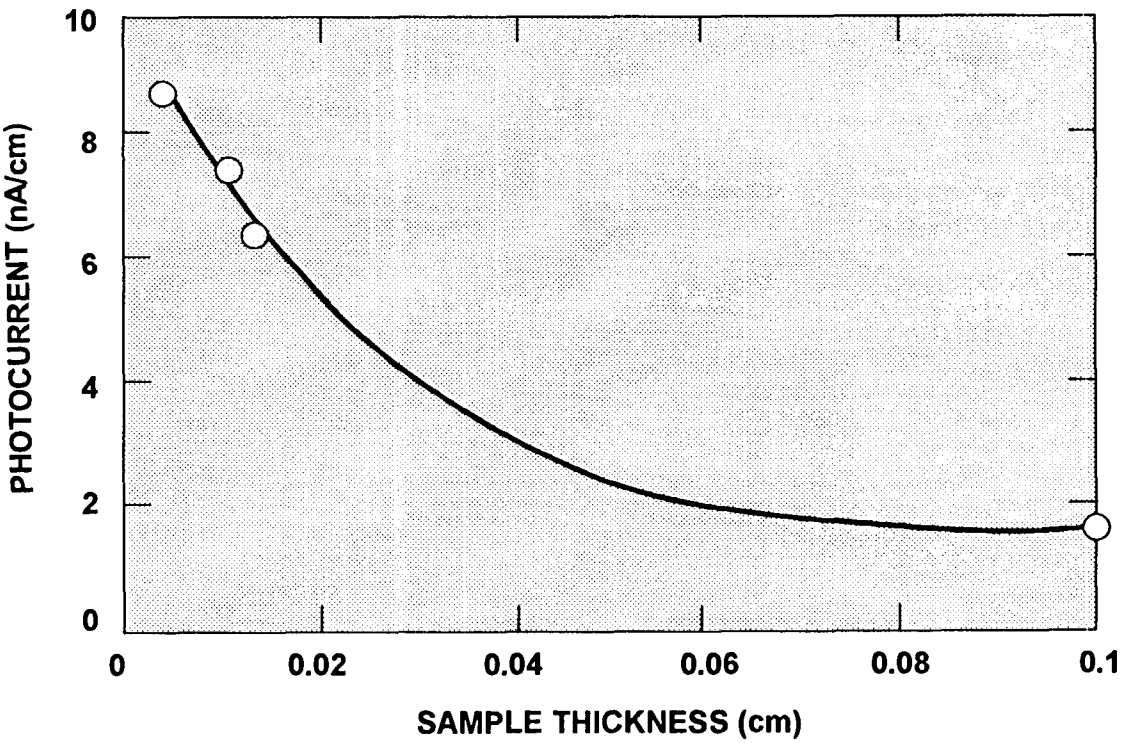

Figure 6: Photocurrent as a function of sample thickness

The relationship between sample thickness and photovoltaic response has been illustrated in Fig. 7. In this model, the absorption coefficient is assumed to be independent of light intensity and the photocurrent density is taken to be proportional to light intensity. The sample is assumed to comprise of thin slices along the thickness direction of the sample. A circuit diagram representing these layers is also shown in the same figure.

The photocurrent flowing through one of the layer of thickness 'dx', located at a distance of 'x' from the sample surface, can be obtained by combining Eq. (1) and (2):

$$di_o = wk\alpha TI_o e^{(-\alpha x)}dx \qquad (3)$$

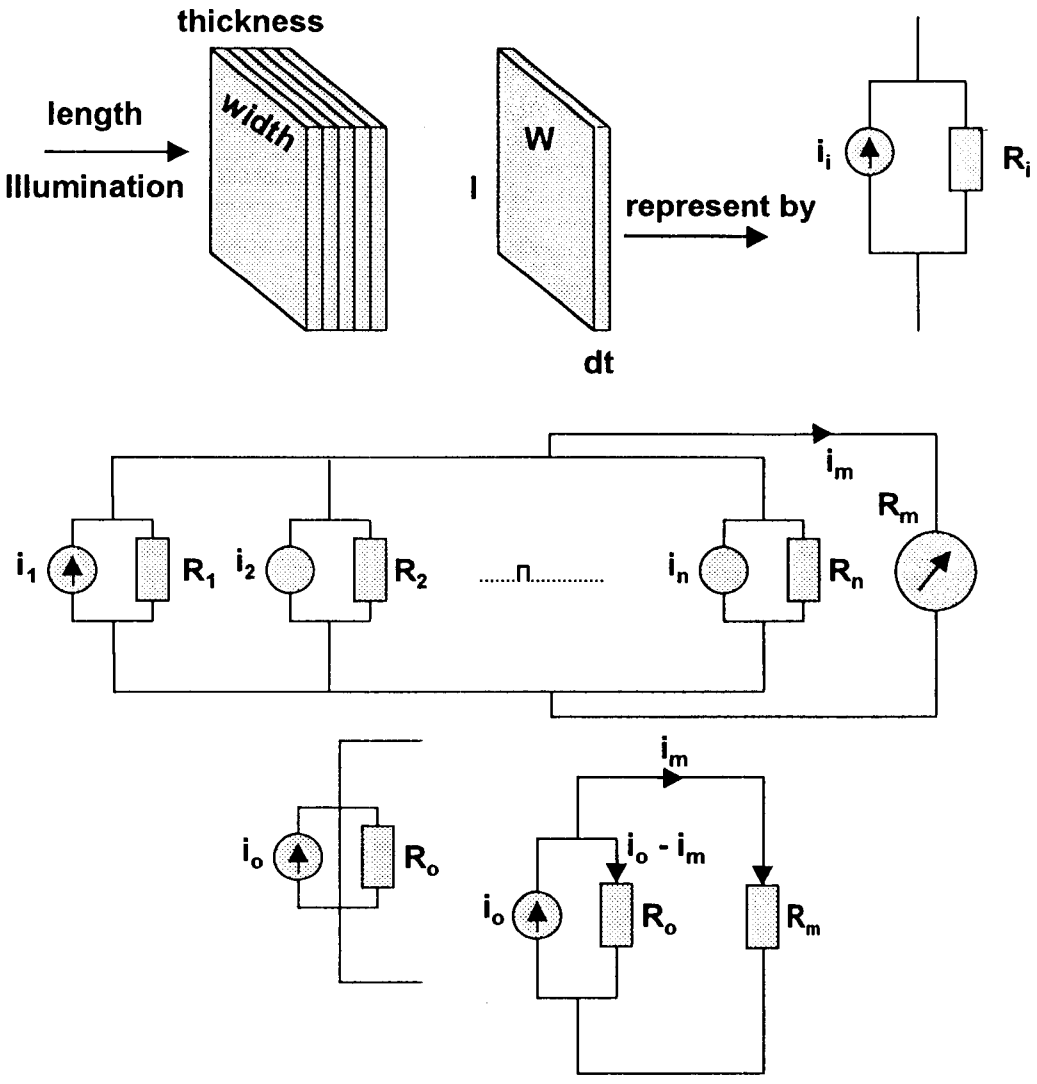

Figure 7: A proposed model for dependence of photocurrent on sample thickness

where di_o is the photocurrent in this layer and w is the sample width. The total photocurrent i_o passing through the sample can be obtained by integrating Eq. (3), over the sample thickness:

$$i_o = \int_0^t wk\alpha TI_o e^{(-\alpha x)} dx = wkTI_o\left(1 - e^{(-\alpha t)}\right) \tag{4}$$

The conductivity of this layer ($\sigma(x)$) can be expressed as a sum of dark conductivity (σ_d) and photoconductivity (σ_{ph}), given as:

$$\sigma(x) = \left(\sigma_d + \sigma_{ph} TI_o e^{(-\alpha x)}\right) \tag{5}$$

The total sample conductance (G_o) (i.e. inverse of resistance) can be obtained by integrating Eq. (5), over the sample thickness.

$$G_o = \frac{1}{R_o} = \int_0^t \frac{w\sigma(x)dx}{L} = \frac{w}{L}\left[\sigma_d t + \frac{\sigma_{ph} T I_o\left(1 - e^{(-\alpha t)}\right)}{\alpha}\right] \tag{6}$$

where L is the electrode gap (length of the sample). In order to measure the photocurrent an external load of resistance R_m was used. The sample and external load are correlated as following:

$$R_o(i_o - i_m) = R_m i_m \tag{7}$$

where i_m is the measured photocurrent and R_m is the external load (Keithley 617) resistance. The Eq. (4), (6) and (7) can be rearranged as:

$$i_m = \frac{wkTI_o\left(1 - e^{(-\alpha t)}\right)}{1 + R_m w\left(\frac{\sigma_d t}{L} + \frac{\sigma_{ph} TIo\left(1 - e^{(-\alpha t)}\right)}{\alpha L}\right)} \tag{8}$$

Fig. 8 shows the plot between i_m (normalized with k) and sample thickness calculated for the external resistance, R_m = 200 TΩ.

As is evident from this figure, with increasing sample thickness, i_m increases, reaches a maxima, and subsequently it decreases with the sample thickness. The optimum thickness (for the current set of samples) which yield maximum photocurrent is found at 33 μm which is about the penetration depth of light. It must be noted that the samples used in this study are thicker than this optimum thickness. It is also reflected in results shown in Fig. 6, where the photocurrent is found to increase with decrease in sample thickness.

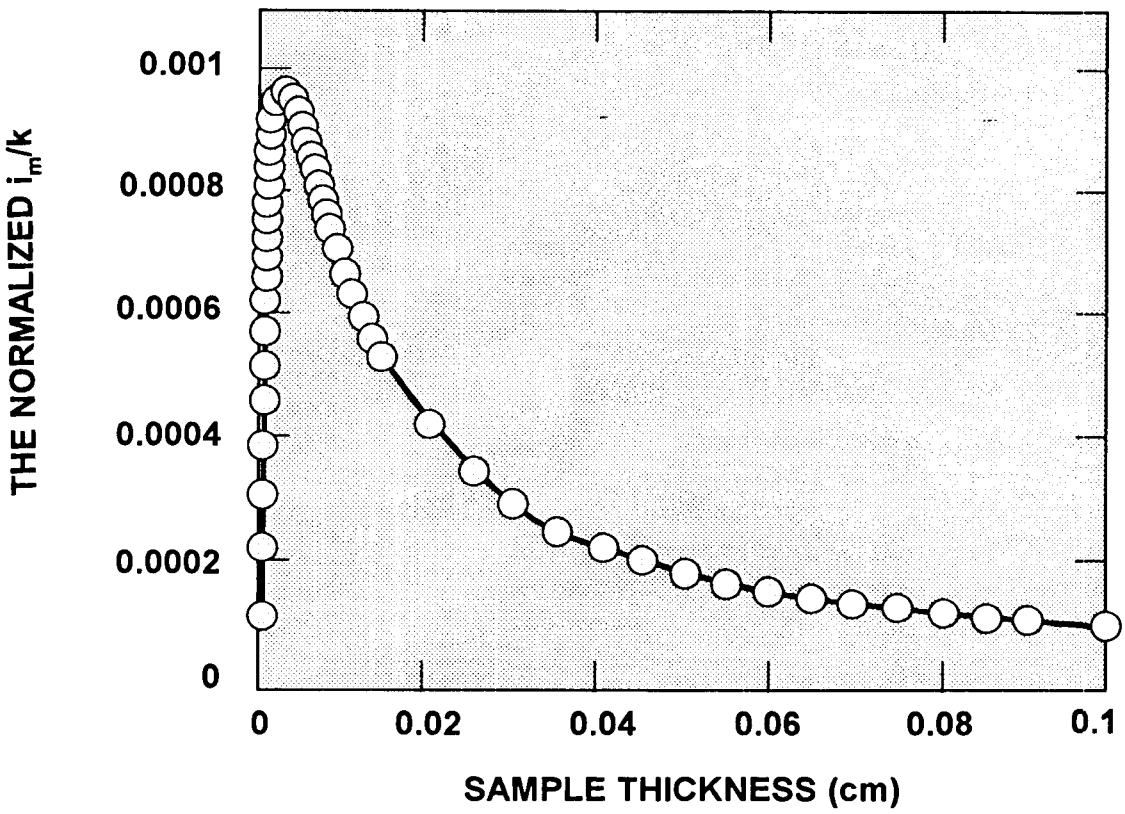

Figure 8: The normalized i_m/k as a function of sample thickness

The results on thickness dependence in the PZT5H composition are summarized in the following table:

Table 4: Thickness Dependence Of Optical Actuation In PZT5H Composition

	THICKNESS microns	RESPONSE mV	DEFLECTION microns	RATIO $D_{ti} / D_{t1=380}$
EXPERIMENTAL DATA				
t_1	380	85	21	1
t_2	200	350	88	4
t_3	165	512	128	6
PROJECTED t_4	33	–	–	20

The results provide confirmation of the analysis summarized in Table 1, and further confirm the projection that optimum film thickness for optical actuation is~ 33 micron with the deflection projected to be ~ 20 times higher than current state of the art wafer of PZT 5H composition at 200 micron thickness.

iv. Optical actuation as function of Surface Roughness for PLZT ceramics:

In order to observe the surface roughness effect, PLZT ceramics (3/52/48) with different surface roughness were prepared by using SiC powder of different grit size followed by final finishing with diamond paste. The surface roughness was measured by a profilometer (Tencor, Alpha-step 200). The average surface roughness was determined using the graphical center line method. Fig. 9 exhibits the photostriction of undoped PLZT as a function of surface roughness.

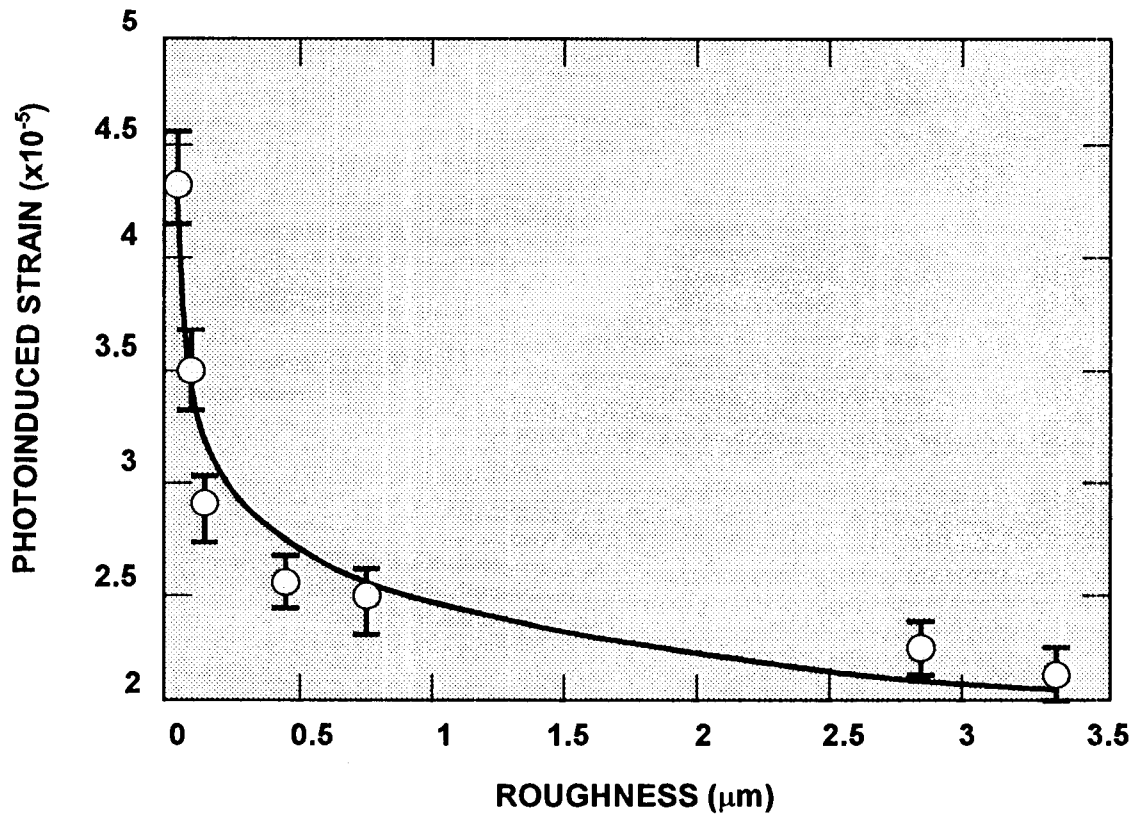

Figure 9: Photoinduced strain as a function of surface roughness

As is evident from this figure, photoinduced strain increases exponentially with the decrease in surface roughness. With increasing surface roughness, the penetration depth of the illumination decreases. This result also reiterates that photostriction is a surface

effect and surface preparation is of extreme importance in the fabrication of high efficiency photostrictive materials.

5. CONCLUSIONS

This work has shown that optical actuation in piezoceramics is indeed a viable option. It will be of particular interest where the actuation control is desired to be contact-less and or remote. The actuation properties of piezoceramics depend sensitively on its composition, structure, thermal history, and surface smoothness/roughness; which offers a broad set of parmeters for optimization of the material and thereby its characteristics. The results provide confirmation of the analysis summarized in Table 1, and further confirm the projection that optimum film thickness for optical actuation is~ 33 micron with the deflection projected to be ~ 20 times higher than current state of the art wafer of PZT 5H composition at 200 micron thickness. Further, choice of suitable flexible substrates is of utmost importance and of course application dependent.

6. ACKNOWLEDGEMENTS

We would like to thank Prof. Eric Cross from Penn State, and Prof. Gene Haertling from Clemson Univ for stimulating discussions regarding actuation. At JPL, we would like to thank Anil Thakoor for providing useful suggestions on this manuscript. The work ~~described in this paper was performed by the Jet Propulsion Laboratory, California Institute of Technology, and~~ was sponsored by the Advanced Concepts Office of National Aeronautics and Space Administration (NASA), and the JPL Director's Research and Development Fund.

7. REFERENCES

1. S.Thakoor, J. A. Cutts, "Flexible Microactuators for Advanced Mobility" New technology report, JPL,.August 1996 NPO # 20019/9651; "Smart Materials for Tiny Robotic Rovers", Science News, 150, p 359 (1996).
2. S. Thakoor, J. M. Morookian, and J. A. Cutts, "Role of Piezoceramic Microactuation for Advanced Mobility", Proceedings of the Tenth IEEE International Symposium on Applications of Ferroelectrics Transactions, Vol 1, pp 205-211, (IEEE Catalog # 96CH35948) .
3. V. M. Fridkin and B. N. Popov, Sov. Phys. Usp. **21,** (1978); M. E. Lines and A. M. Glass, Principles and Applications of Ferroelectrics and Related Materials (Clarendon, Oxford, 1977), Chaps., 5,12, and 16; K. Uchino, Y. Miyazawa, and S. Nomura, Jap. J. of Appl. Phy., Vol 22, 102, Dec 1983; " Capturing Sound Light and Strength with New Materials", Meeting Briefs, Science, **266**, Dec 1994.
4. A. J. Moulson & J. M. Herbert, Electroceramics, chapman & Hall Publishers, 298 (1992).

5. A. F. Flynn et al., Journal of Microelectromechanical Systems, **1**, 44, (1992); A. F. Flynn, Ph. D Thesis, MIT(June, 1995); R. Gerson and T. C. Marshall, J. of App. Phy., **30**, 1650 (1959).
6. S. Thakoor and A. Stoica: "Biomorphic Explorers" New Technology Report, February 1997, NPO# 20142/9778; K. Uchino, J. Rob. Mech., 1, 124 (1989); T. Fukuda, S. Hattori, F. Arai, H. Matsuura, T. Hiramatsu, Y. Ikeda, A. Maekawa, Rob. Automation, **2**, 618, (1993); K. Uchino, "New Applicaitons of Photostriction," *Innovations in Materials Research*, Vol. 1, No. 1, pp. 11-22, 1996.
7. P. Poosanaas, A. Dogan, A.V. Prasada Rao, K. Komarneni and K. Uchino, "Photostriction of Sol-Gel Processed PLZT Ceramics," *J. Electroceramics*, Vol. 1, No. 1, pp. 105-111, 1997.
8. S. Thakoor, and J. Maserjian, "Photoresponse Probe of the space charge distribution in Ferroelectric PZT thin film memory capacitors" J. Vac. Sci. &Tech A, **12** , 295, Mar/April(1994); S. Thakoor, "High Speed, Optoelectronic Response from the Edges of lead Zirconate Titanate Thin Film Capacitors", Appl. Phy. Lett. **63**(23), 3233, 1993
9. S. Thakoor, US patent # 5196101, March 23, 1993.
10. A. Yavrovian, S. P. S. Yen, G. Plett and N. Weissman; High temperature Materials for Venus Balloon Envelopes, Proc. 11th AIAA Lighter than air system technology Conference held May 16-18 1995, Clear water Florida.
11. N. Marzwell, Internal communication, April 1997.
12. M. Glass, D. von der Linde, D. H. Auston, and T. J. Negran, "Excited State Polarization, Bulk Photovoltaic Effect and the Photorefractive Effect in Electrically Polarized Media," *Electronic Materials*, Vol. 4, No. 5, pp. 915-943, 1975.